

Article

Diagnostics of Interior PM Machine Rotor Faults Based on EMF Harmonics

Natalia Radwan-Pragłowska *  and Tomasz Wegiel 

Faculty of Electrical and Computer Engineering, Cracow University of Technology, Warszawska 24 St., 31-155 Cracow, Poland; tomasz.wegiel@pk.edu.pl

* Correspondence: natalia.radwan-pragłowska@pk.edu.pl

Abstract: This article presents a detailed study on the diagnosis of rotor faults in an Interior Permanent Magnet Machine based on a mathematical model. The authors provided a wide literature review, mentioning the fault diagnosis methods used for Permanent Magnet Machines. The research emphasizes the necessity of precise assumptions regarding winding construction to accurately analyze the additional harmonics appearing in rotor faults caused by electromotive force (EMF), i.e., rotor eccentricity and magnet damage. The article also discusses specific features appearing in the spectrum of air gap permeance functions and the impact of rotor eccentricity and magnet damage on PM flux density distribution and as a consequence on EMF stator windings. The novelty of the presented content is the analysis of induced EMFs for cases of the simultaneous occurrence of rotor eccentricity and PM damage. The findings of this study provide valuable insights for the diagnosis and understanding of internal asymmetries in Interior PM Machines.

Keywords: permanent magnet machines; rotor faults; eccentricity; PM damage



Citation: Radwan-Pragłowska, N.; Wegiel, T. Diagnostics of Interior PM Machine Rotor Faults Based on EMF Harmonics. *Energies* **2024**, *17*, 2198. <https://doi.org/10.3390/en17092198>

Academic Editor: Youguang Guo

Received: 21 March 2024

Revised: 26 April 2024

Accepted: 30 April 2024

Published: 3 May 2024



Copyright: © 2024 by the authors. Licensee MDPI, Basel, Switzerland. This article is an open access article distributed under the terms and conditions of the Creative Commons Attribution (CC BY) license (<https://creativecommons.org/licenses/by/4.0/>).

1. Introduction

Permanent Magnet Synchronous Machines (PMSMs) are crucial in many industrial and automotive applications, particularly in electric and autonomous vehicles. The reliability and efficiency of these motors directly impact the overall performance and safety of the systems they power. An example of an Interior PM motor used in electric vehicles is the Prius Motor. The literature on the electric motor of the Toyota Prius highlights the significant advancements and ongoing challenges in the field of hybrid vehicle technology [1–3]. The evolution from early electric vehicles to sophisticated hybrids like the Prius reflects a blend of engineering innovation and environmental consideration. As the automotive industry continues to evolve towards more sustainable solutions, research on electric motors and their application in hybrid vehicles will remain a critical area of study. The Toyota Prius utilizes an Interior Permanent Magnet Synchronous Motor, known for its efficiency and compact design, making it suitable for HEVs (Hybrid Electric Vehicles) [4,5]. The use of PMSMs and their impact on the performance and efficiency of the Prius is a significant area of study.

As such, detecting faults and ensuring optimal operation are vital aspects of PMSM technology. Numerous studies have been conducted on the diagnosis of internal asymmetry in PM machines [6–11]. Such faults can significantly impact the motor's performance, leading to inefficiencies, reduced torque output, and even complete system failures. Also, the review presented in [12] provides a comprehensive review of faults in Permanent Magnet Synchronous Motors and their diagnostic methods. PMSM faults are categorized into electrical, mechanical, and magnetic types, each with distinct characteristics and implications. This paper thoroughly examines various fault diagnosis methods, including model-based, signal processing, and data-driven intelligent diagnostic algorithms. These methods range from traditional model-based approaches to advanced techniques like

neural networks and deep learning, highlighting their applicability and effectiveness in identifying and addressing different PMSM faults.

The PMSM faults can be divided into three categories. The first one covers stator winding faults, which are critical issues that can adversely affect the motor's performance. These are generally classified into a few main forms:

- Short circuit faults, which occur when there is an electrical connection between two points in the winding that should not be connected (inter-turn—within the same winding, phase-to-phase—between two different windings, or winding-to-ground);
- Open circuit faults—the open circuit in the stator winding is essentially a break in the winding, and this could be due to a broken conductor or a poor soldering joint;
- Winding deformation—this is less of a fault and more a result of operational stress.

Studies on diagnosing stator winding are presented in several publications. The study performed in [13] describes a comprehensive approach for detecting faults in the stator winding of PMSMs. This research focuses on three common faults: Unbalanced Winding Resistance (UWR), Turn-to-Turn Short Circuit (TSC), and Phase-to-Phase Short Circuit (PSC). The methodology involves using an Artificial Neural Network (ANN) to classify these faults, demonstrating a high accuracy rate of 98.5% in fault detection. The study highlights the dependence of fault indicators on operating points and the severity of faults, advocating for a data-driven diagnostic approach that considers these variables. In [14] the authors present an innovative approach for detecting stator inter-turn short circuit faults in PMSM. The authors introduce a time-frequency method utilizing an improved wavelet packet transform to analyze both the stator current signal and vibration signal for fault detection. This research is significant due to the prevalence of PMSMs in various industrial applications and the critical impact of motor faults on production and efficiency.

Also, a comprehensive study on diagnosing stator winding faults in Permanent Magnet Synchronous Motors using stator phase current analysis is presented in [15]. It explores various methods, including Fast Fourier Transform (FFT) and Discrete Wavelet Transform (DWT), for identifying Inter-Turn Short Circuits (ITSCs) in PMSMs. In [16], the same authors present a study on diagnosing demagnetization faults in PMSMs using stator current signal processing and machine learning algorithms.

Another group of Permanent Magnet Synchronous Motor damage includes demagnetization faults (magnet damage). Demagnetization faults in PMSMs refer to the reduction or loss of magnetic strength in the rotor's permanent magnets. This phenomenon significantly affects the performance and efficiency of the motor. The review from [17] covers a broad spectrum of methodologies and discusses the advantages and disadvantages of different diagnostic methods, providing a comparative analysis and a synthesis of various research studies. The diagnosis methods for demagnetization faults in Permanent Magnet Synchronous Motors, as outlined in the document, can be categorized into two main groups: software-based (like Finite Element Method (FEM), Frequency Domain Analysis, or Field Reconstruction Method (FRM)) [18] and hardware-based methods (like, among others, Fast Fourier Transform (FFT) of stator components (zero sequence currents, voltage, and current), time frequency transform of stator components, analysis based on noise, vibration and torque, measurement of the zero sequence voltage components (the spectrum of the back-EMF)) [19]. These methods represent a comprehensive approach to monitoring and diagnosing PMSMs, each with its unique advantages and applications. The choice of method depends on the specific requirements of the diagnosis, such as the type of fault to be detected, the precision needed, and the available resources for the diagnosis process.

The research in [18] is focused on detecting such faults and highlights the significant impact of magnet failures on motor performance. The authors propose a diagnostic method based on measuring the Zero Sequence Voltage Component (ZSVC), which is suitable for inverter-fed machines and particularly useful for fault-tolerant systems. In [20], the authors also focused on PMSM operations under demagnetization, showing the impact of demagnetization on the current spectrum of PMSMs, with the ultimate goal of developing an effective monitoring system for these conditions. The researchers employed both simu-

lation and experimental approaches, harnessing a two-dimensional finite-element analysis (FEA). They effectively applied continuous wavelet transform (CWT) and discrete wavelet transform (DWT) methods to detect and discriminate demagnetization faults in PMSM motors under nonstationary conditions. The next article [21] focuses on the diagnostic techniques for identifying demagnetization faults in direct-drive permanent magnet machines. They compare the efficacy of three different methods, Current Signature Analysis (CSA), Park's Vector Approach (PVA), and Extended Park's Vector Approach (EPVA), in detecting these faults. In [22], the authors present a comprehensive study on detecting permanent magnet damage in Permanent Magnet Synchronous Motors using Convolutional Neural Networks (CNNs). The focus is on directly analyzing stator phase currents to identify PM faults. The publication [23] introduces the Angular Domain Order Tracking (AD-OT) method as a novel approach to diagnose demagnetization faults in PMSMs. This method monitors the motor phase current under various speed and load conditions, including both stationary and non-stationary rotor speeds. The results obtained from the AD-OT method are compared with those from the traditional Fast Fourier Transform (FFT) approach. The article [24] presents a novel method for diagnosing rotor demagnetization and eccentricity faults in Interior Permanent Magnet Synchronous Motors using deep Convolutional Neural Networks (CNNs) and image recognition. This approach transforms stator current data into grey images using an autocorrelation matrix, enhancing feature representation for fault detection.

The further discussion, also focusing on the issue of demagnetization in PM machines, especially in renewable energy applications like wind, tidal, and wave energy, is contained in [25]. The paper presents a detailed analysis of demagnetization in PM machines using a direct-drive C-GEN permanent magnet generator. The paper presents the impact of demagnetization on the generator's harmonic index, the spatial distribution of demagnetization, and its effect on multiple generator stages. This includes exploring the impact of circulating currents due to faults and the resulting additional thermal stress. The related article [26] discusses the issue of partial demagnetization in PM machines, which can occur due to overloading or thermal stress. This demagnetization leads to asymmetry in the air-gap field, causing harmonics that result in extra losses, mechanical oscillations, and reduced efficiency. The authors present an analytical investigation of the expected harmonics in the stator current spectrum in the case of demagnetization, considering factors like stator winding and the number of poles. The analyses are verified by FEA simulations and experimental tests.

The next group of motor faults are the eccentricity faults, involving static eccentricity (SE) and dynamic eccentricity (DE), which are critical issues in PMSMs. Static eccentricity occurs when there is a constant offset of the rotor's center from the stator's center. Dynamic eccentricity, on the other hand, involves a variation in the rotor-stator gap as the rotor turns. The analysis and mitigation of eccentricity in PMSMs are crucial for ensuring the longevity, efficiency, and reliability of these motors. The research in [27] delves into the recognition of these faults using Stator Current Signature Analysis (SCSA). The study proposes a frequency pattern for eccentricity fault recognition, which remains unaffected by load variation, a common challenge in fault detection. Wavelet analysis is employed for feature extraction, considering both stationary and non-stationary signals in PMSMs. The methodology shows a strong correlation between different degrees of SE and DE with the amplitude of sideband components, enabling accurate fault detection. Furthermore, the application of Principal Component Analysis (PCA) and k-Nearest Neighbors (k-NN) classification demonstrates the method's efficacy in identifying and estimating the degree of eccentricity faults, even in the presence of measurement noise. The integration of ANN, back-EMF analysis, wavelet transform, PCA, and k-NN classification in the above studies presents a comprehensive and effective approach for diagnosing faults in PMSMs. These methodologies offer significant improvements in accuracy, reliability, and cost-effectiveness for fault detection systems, crucial for the maintenance and performance optimization of PMSMs. One article [28] contains the novel method that incorporates

the effects of stator slots and saturation in diagnosing static and dynamic eccentricity faults. Eccentricity faults are also presented in [29], where the authors present a method for diagnosing static eccentricity faults in external rotor permanent magnet synchronous motors (ER-PMSM), particularly as used in in-wheel motor applications. In this paper, a novel diagnostic approach based on the Total Harmonic Distortion (THD) of no-load Back-EMF is proposed. This method involves using intersection lines for SE fault diagnosis, allowing for the detection of both the SE ratio and SE circumferential angle. Also, [30] describes the rotor faults, focusing on detecting three categories of faults: static eccentricity, dynamic eccentricity, and flux disturbances due to permanent magnet defects.

Initially, it might seem that the topic has been thoroughly addressed and adequately described [31,32]; however, deeper analyses indicate the need to clarify the assumptions regarding the winding construction for the formulas related to the appearance of additional harmonics in the EMF, in cases of rotor eccentricity and PM damage (demagnetization).

Referring to the commonly known Motor Current Signature Analysis MCSA method, it should be noted that the reason for the generated additional harmonics in the stator current spectrum is the appearance of additional harmonics in the induced stator phase voltages in the no-load state (EMF). For example, in works [17,18,20,23], additional components appearing in the EMF spectrum for cases of magnet damage (demagnetization) have pulsations $(1 \pm \frac{h}{p})p\Omega$ (where $h = 0, 1, 2, \dots$; p —number of pole pairs; Ω —rotational speed). Other publications [12,27–29] provide a formula for the appearance of additional pulsations in the EMF spectrum in the case of eccentricity in the following form $(1 \pm \frac{2h-1}{p})p\Omega$. Publications [25,26] refine the previously presented relationships and provide a certain modification of the formulas determining additional pulsations in the EMF spectrum for cases of damage caused by demagnetization, but they are not universal, as they mostly apply to machines with concentrated windings. To sum up, it can be said that the above commonly used formulas work well for the construction of machines with a relatively small number of slots and a relatively large number of pole pairs. These are usually winding designs with a fractional number of slots per pole and phase. Due to the above doubts, the authors of this article decided to clarify these issues by using an analytical mathematical model for a PM machine with internal magnets, based on the analysis of the spatial harmonics of the magnetic field in the air gap of the machine in cases of rotor damage related to the eccentricity and demagnetization of magnets.

The main goal of the presented approach is to use an analytical model that allows for an effective analysis of stator-winding-back EMF. This approach is competitive with FEM calculations and provides the possibility of synthesizing electromagnetic phenomena in machines. In addition, analytical calculations are much simpler, faster and, above all, cheaper. For this purpose, a PM mathematical model of the machine was developed, allowing for the inclusion of any type of three-phase stator winding. Based on this model, it will be possible to qualitatively and quantitatively determine the pulsations occurring in the EMF spectrum for cases of simultaneous and separate occurrence of rotor damage, such as static, dynamic, mixed eccentricities and demagnetization. A certain novelty presented in the article is the methodology of modeling PM damage with the simultaneous occurrence of rotor eccentricity. The verification of the correctness of the created analytical model will be presented by FEM analyses for an example electric motor structure from a Toyota Prius.

2. Mathematical Model for Diagnostic Purposes

2.1. General Assumptions

The assumption of linearity of the magnetic circuit is the key element for further analyses contained in the paper (characteristic of PM: $B_m = B_r + \mu_0\mu_r H_m$). This assumption in PM machines is usually acceptable [33,34]. Windings can then be described by flux

linkage excited by PM, which is also a function of the rotation angle φ . The EMF of a three-phase PM machine can be written in a standard matrix form:

$$\frac{d}{dt} \Psi_{\text{PM}}(\varphi) = \omega \begin{bmatrix} \frac{\partial \psi_{\text{PM}1}(\varphi)}{\partial \varphi} \\ \frac{\partial \psi_{\text{PM}2}(\varphi)}{\partial \varphi} \\ \frac{\partial \psi_{\text{PM}3}(\varphi)}{\partial \varphi} \end{bmatrix} = \mathbf{e}_{\text{PM}} = \begin{bmatrix} e_{\text{PM}1} \\ e_{\text{PM}2} \\ e_{\text{PM}3} \end{bmatrix} \quad (1)$$

where $\psi_{\text{PM}a}(\varphi)$ —flux linkage of winding "a" ($a = 1, 2, 3$), produced by PMs, and $e_{\text{PM}a}$ —EMF of winding "a" ($a = 1, 2, 3$), produced by PMs.

Generally, when we consider the non-regular shape of the magnetic circuit according to the eccentricity and faults of magnets, the vector of PM flux linkages can be presented as

$$\Psi_{\text{PM}}(\varphi) = \sum_{n=\pm 1, \pm 2, \pm 3, \dots} \Psi_n^{\text{PM}} \cdot e^{jn\varphi} \quad (2)$$

The specific features of PM machines allow an approach often used to calculate the flux linkage of windings based on the basis of field radial component distribution in the air gap. The variability of linkage fluxes must also be specified as a function of rotation angle in a zero-current state. The following subsections present the designation of analytic EMF dependences of PM machines.

2.2. EMF Induced by PM in Cases of Rotor Faults

2.2.1. Flux Density Distribution in the PM Machine Air Gap

For analysis, an example cross-section of a synchronous machine with permanent magnets, shown in Figure 1, was considered. We assumed that the length of the magnetic flux lines in the air gap and magnet were equal, respectively, to the lengths of the magnet and air gap, which is a consequence of the assumption to take into account only the radial component of the magnetic field.

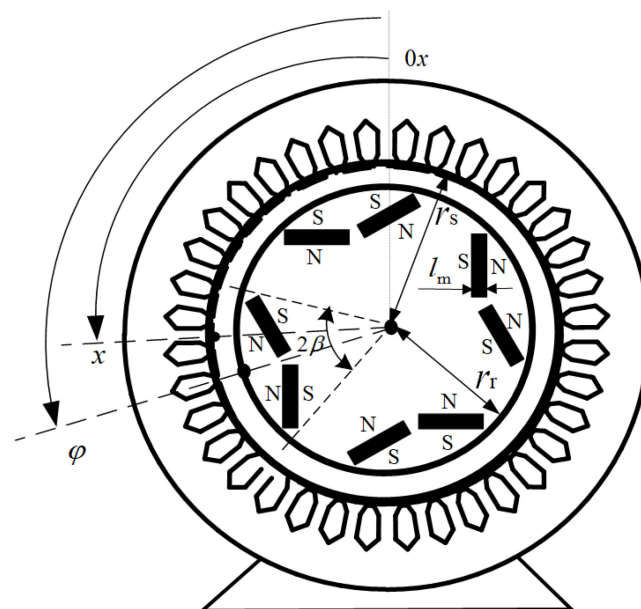


Figure 1. A simplified cross-section of an interior PM machine.

For the model of the one-dimensional distribution of the magnetic field in the machine, which assumes the presence of only a radial component, that the flux density in the air gap is, in general, a function of two variables (depending on the location on the periphery of

the gap x and the angle of rotation of the rotor φ), and that its components depend on the arrangement of permanent magnets in the magnetic circuit [34,35].

$$B_{PM}(x, \varphi) = \frac{\lambda_{\delta}(x, \varphi)}{\lambda_g} B_m(x - \varphi) - B_0^{PM} \tag{3}$$

where $B_{PM}(x, \varphi)$ —radial component of flux density in the air gap excited by PMs, $B_m(x, \varphi)$ —distribution of flux density in the air gap excited by PMs for the case of a machine with a cylindrical smooth air gap, $\lambda_{\delta}(x, \varphi)$ —permeance function of air gap, and λ_g —unit permeance value of a symmetrical and slot-less air gap ($\lambda_g = \frac{\mu_0}{l_{\delta}}$; $l_{\delta} = r_s - r_r$).

Based on the law of source-lessness of the magnetic field $\int_x^{x+2\pi} B_{PM}(x', \varphi) dx' \equiv 0$, there is a condition that must be taken into account in further entries; hence, in Equation (3), B_0^{PM} is a constant component of the product of the function $B_m(x, \varphi)$ and the permeance of the air gap. Modeling the real shapes of the air gap is possible using the air gap permeance function [36–40].

$$\lambda_{\delta}(x, \varphi) = \frac{\mu_0}{\delta_{\delta}(x, \varphi)} = \frac{\mu_0}{\delta(x, \varphi) + \Delta\delta_s(x, \varphi)} \tag{4}$$

The permeance function is proportional to the inverse of the length of the magnetic field force lines (Figure 2), which can be approximated for the air gap as follows; $\delta_{\delta}(x, \varphi) = \delta(x, \varphi) + \Delta\delta_s(x, \varphi)$, where $\delta(x, \varphi)$ is a function of the equivalent lengths of the magnetic field lines for the air gap.

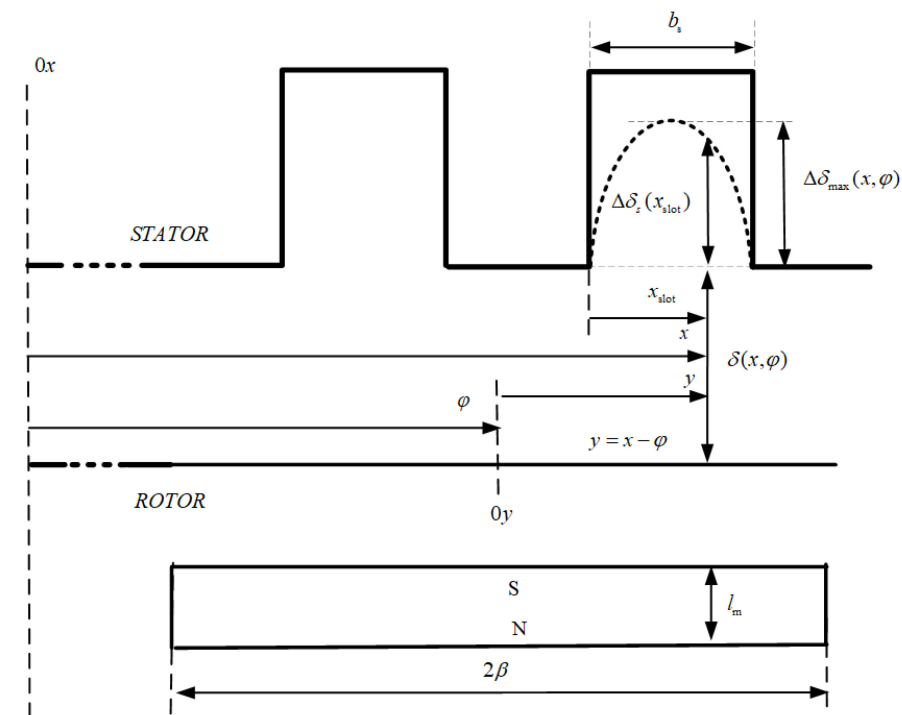


Figure 2. Explanation of the calculation of magnetic line lengths.

The slots on the side of the stator surface additionally modify the lengths of the magnetic field lines. Therefore, correction values should be added in appropriate places around the circumference of the air gap $\Delta\delta_s$. The magnitudes of the above-mentioned corrections can be determined using analytical relationships from the conformal mapping

method to model the magnetic field over the groove, similar to the derivation of the Carter coefficient [36,38–40].

$$\Delta\delta_s(x, \varphi) = \begin{cases} \Delta\delta_{\max}(x, \varphi) \sin(\frac{\pi}{b_s} x_{\text{slot}}) & \text{for slots} \\ 0 & \text{for teeth} \end{cases} \quad (5)$$

where b_s is an equivalent slot opening, x_{slot} is a local variable over a slot $x_{\text{slot}} \in (0, b_s)$, and $\Delta\delta_{\max}(x, \varphi)$ —maximum value of the correction of the length of the magnetic field lines in the slot determined using the formulas [35,36,40] presented in Appendix A.

For a symmetrical air gap without taking into account slots, the function $\delta(x, \varphi) = l_\delta = r_s - r_r$ is constant.

In general, Fourier coefficients of permeance functions $\lambda_\delta(x, \varphi)$ are obtained using the 2D FFT algorithm with respect to two variables, x and φ .

$$\lambda_\delta(x, \varphi) = \sum_{m \in M_\delta} \sum_{n \in N_\delta} \lambda_{m,n}^\delta e^{jmx} e^{jn\varphi} \quad (6)$$

The unit permeance function (6) contains harmonics whose order belongs to the set of integers. The maximum number of permeance harmonics depends on the shape and asymmetry of the air gap [38–40].

The proposed approach to modeling the permeance function also makes it possible to take into account the rotor eccentricity by correcting the length of the magnetic field lines in the air gap $\delta(x, \varphi)$, which is explained in Appendix B.

For magnets without damage and symmetrically located, the distribution of flux density in the air gap for a symmetrical, slot-less air gap in the zero current state can be written as $B_m(x - \varphi) = B_m^{\text{sym}}(x - \varphi)$, according to Figure 3.

$$B_m^{\text{sym}}(x - \varphi) = \sum_{\zeta \in Q} B_\zeta^m \cdot e^{j\zeta(x-\varphi)} \quad (7)$$

$$B_\zeta^m = \frac{2}{\pi} \frac{B_0}{\zeta} p \sin(\zeta \beta) \quad B_0 = B_r \frac{l'_m}{l'_m + l_\delta} \quad Q = \{-\zeta_{\max} \dots -5p, -3p, -p, p, 3p, 5p \dots \zeta_{\max}\} \quad (8)$$

where l_m —magnet thickness and $l'_m = \frac{l_m}{\mu_{rm}}$.

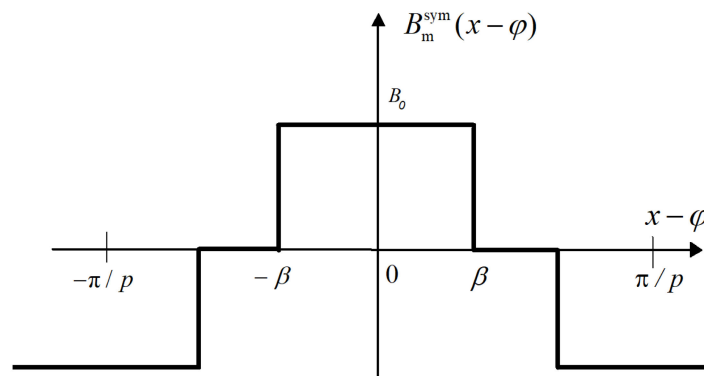


Figure 3. PM flux density distribution in the air gap for symmetrical and slot-less machines.

For asymmetrical magnets $B_m(x - \varphi) = B_m^{\text{dem}}(x - \varphi)$, e.g., with damaged poles as a result of demagnetization, the function describing the distribution of flux density in the air gap for the case of symmetrical magnets $B_m^{\text{sym}}(x - \varphi)$ should be corrected using the function modeling the damage $D_{\text{PM}}(x - \varphi)$.

$$B_m^{\text{dem}}(x - \varphi) = B_m^{\text{sym}}(x - \varphi) \cdot D_{\text{PM}}(x - \varphi) \quad (9)$$

In the case of damage to one magnetic pole, the function $D_{PM}(x - \varphi)$ can be presented in accordance with Figure 4, and in the case of damage to a pair of magnetic poles, it can be presented in accordance with Figure 5.

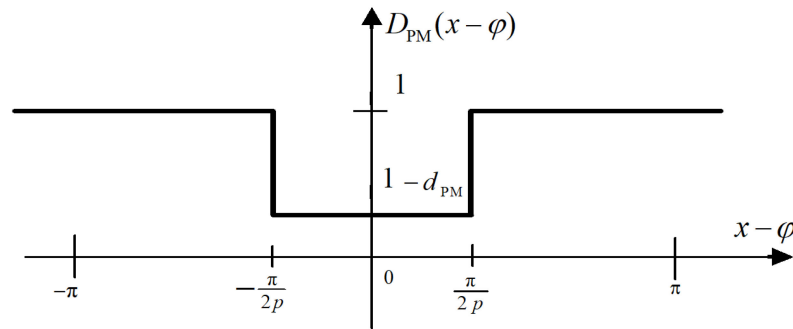


Figure 4. Modeling damage to one magnetic pole.

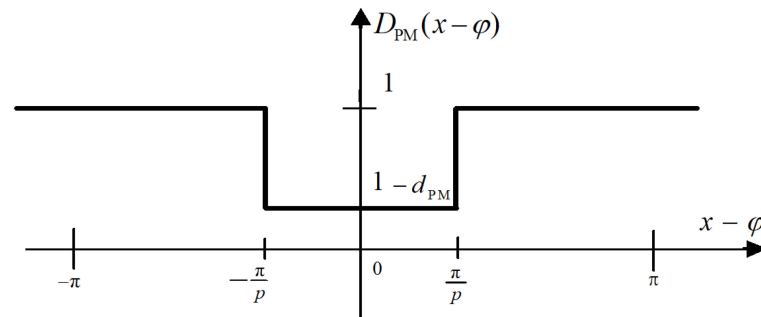


Figure 5. Modeling damage to one pair of magnetic poles.

The degree of PM damage is determined by the coefficient $d_{PM} \in [0; 1]$ ($d_{PM} = 0$ no demagnetization, $d_{PM} = 1$ full demagnetization). Generally, the demagnetization modeling function $D_{PM}(x - \varphi)$ can be presented in the form of a Fourier series and is qualitatively the same for both of the damage cases.

$$D_{PM}(x - \varphi) = \sum_{k \in K \dots} D_k^{PM} \cdot e^{jk(x - \varphi)} \tag{10}$$

where set $K = \{-k_{max} \dots -3, -2, -1, 0, 1, 2, 3 \dots k_{max}\}$, while the series coefficients are as follows:

<p>Magnetic pole damage</p> $D_k^{PM} = \begin{cases} \frac{2p - d_{PM}}{2p} & \text{for } k = 0 \\ -\frac{d_{PM}}{\pi k} \sin(k \frac{\pi}{2p}) & \text{for } k \neq 0 \end{cases}$	<p>Damage to one pair of magnetic poles</p> $D_k^{PM} = \begin{cases} \frac{p - d_{PM}}{p} & \text{for } k = 0 \\ -\frac{d_{PM}}{\pi k} \sin(k \frac{\pi}{p}) & \text{for } k \neq 0 \end{cases}$	(11)
--	---	------

It should be added that for the analysis of magnetic field distributions in the air gap, it is necessary to reject the constant component, which is related to the source-less condition of the magnetic field; therefore,

$$B_m(x - \varphi) = B_m^{dem}(x - \varphi) = B_m^{sym}(x - \varphi) \cdot D_{PM}(x - \varphi) = \sum_{\zeta \in Q} \sum_{k \in K} B_{\zeta, k}^m e^{j(\zeta + k)(x - \varphi)} \tag{12}$$

where

$$B_{\zeta k}^m = \begin{cases} B_{\zeta}^m \cdot D_k^{PM} & \text{for } \zeta + k \neq 0 \\ 0 & \text{for } \zeta + k = 0 \end{cases} \tag{13}$$

For the special case of the symmetry of magnets, the coefficient $d_{PM} = 0$ and the set $K = \{0\}$ and function $D_{PM}(x - \varphi) \equiv 1$.

Taking into account the above derivations and the condition of source-lessness of the magnetic field, we obtained the distribution function of the induction caused by PM in the air gap of the machine, also taking into account the asymmetry of the magnetic circuit caused by the eccentricity of the rotor and damage to the magnets.

$$B_{PM}(x, \varphi) = \sum_{\zeta \in Q} \sum_{k \in K} \sum_{m \in M_s} \sum_{n \in N_s} B_{\zeta, k, m, n}^{PM} e^{j(\zeta+k+m)x} e^{j(-\zeta-k+n)\varphi} \quad (14)$$

where

$$B_{\zeta, k, m, n}^{PM} = \begin{cases} B_{\zeta}^m \cdot D_k^{PM} \frac{\lambda_{m, n}^s}{\lambda_g} & \text{for } \zeta + k \neq 0 \wedge \zeta + k + m \neq 0 \wedge -\zeta - k + n \neq 0 \\ 0 & \text{for opposed condition} \end{cases} \quad (15)$$

2.2.2. PM Flux Linkages and EMF of Windings

In order to determine the characteristics of the windings, i.e., Magneto-Motive Force MMF relationships, it was assumed that the windings “a” and “b” (Figure 6), with the number of turns, respectively, w_a and w_b , are characterized by winding factors $k_{wa}^{|\nu|}$, $k_{wb}^{|\nu|}$ and produce MMFs:

$$\Theta_a(x) = \sum_{\nu \in P_a} \Theta_{\nu}^a e^{j\nu(x-x_a)}; \quad \Theta_b(x) = \sum_{\nu \in P_b} \Theta_{\nu}^b e^{j\nu(x-x_b)} \quad (16)$$

where

$$\Theta_{\nu}^a = i_a \frac{1}{\pi} W_{\nu}^a, \quad \Theta_{\nu}^b = i_b \frac{1}{\pi} W_{\nu}^b; \quad W_{\nu}^a = \frac{w_a k_{wa}^{|\nu|}}{|\nu|}; \quad W_{\nu}^b = \frac{w_b k_{wb}^{|\nu|}}{|\nu|} \quad (17)$$

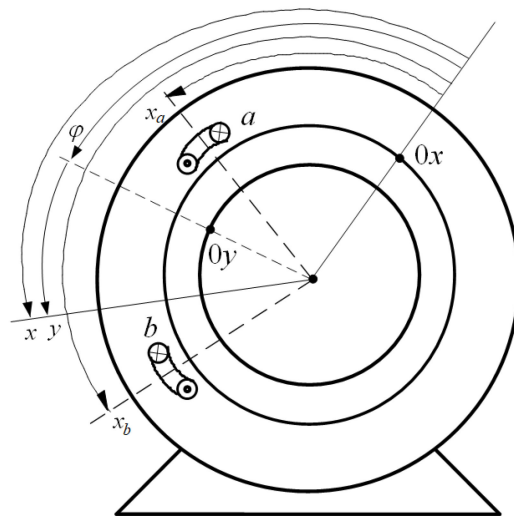


Figure 6. A simplified model illustrating the location of the windings of a PM machine.

Fourier spectra of winding MMFs contain harmonics “ ν ” belonging to sets P_a and P_b . The contents of these sets are as follows:

- $P = P^{qc} = \{-\nu_{max} \dots -5p, -3p, -p, p, 3p, 5p \dots \nu_{max}\}$ —winding with the integer number of slots per pole and phase;
- $P = P^{qf} = \{-\nu_{max} \dots -5p, -4p, -3p, -2p, -p, p, 2p, 3p, 4p, 5p \dots \nu_{max}\}$ —winding with a fractional number of slots per pole and phase.

For three-phase winding, the positions of the magnetic axes of the windings are

$$x_a = (a - 1) \frac{2\pi}{3p}, \quad x_b = (b - 1) \frac{2\pi}{3p} \text{ for } a, b = 1, 2, 3. \quad (18)$$

The flux linkage ψ_a with the “a” winding, according to [37,40], can be expressed as the sum of the flux linkage of the elementary windings distributed sinusoidally for subsequent harmonics, which can be written as follows

$$\psi_a(\varphi) = \sum_{\nu \in P_a} \int_{-l_c/2}^{l_c/2} \left\{ \int_{x_a - \pi/|\nu|}^{x_a} \left[g_\nu^a(x) \cdot \sum_{k=1}^{|\nu|} \left(\int_{x+2\pi(k-1)/|\nu|}^{x+\pi/|\nu|+2\pi(k-1)/|\nu|} [B(x', \varphi) r_s] dx' \right) \right] dx \right\} dz \quad (19)$$

where $g_\nu^a(x) = \frac{1}{l_a} \frac{d\Theta_\nu^a}{dx} = j \frac{\nu}{\pi} W_\nu^a e^{j\nu(x-x_a)}$ —distribution of turn density for the ν -th harmonic of the winding “a”; $B(x, \varphi)$ —distribution of the radial component of flux density in the air gap on the stator surface; and l_c —equivalent axial length of the machine.

For the assumed arbitrary distribution of magnetic field in the form

$$B(x, \varphi) = \sum_{\zeta} B_\zeta(\varphi) \cdot e^{j\zeta x} \quad (20)$$

and to perform the integrations appearing in expression (19), the following relationship is obtained:

$$\psi_a(\varphi) = \sum_{\zeta \in P_a} 2r_s \cdot l_c \cdot W_\nu^a \cdot B_{-\zeta}(\varphi) \cdot e^{-j\zeta x_a} \quad (21)$$

which shows that the flux linked to the winding consists only of spatial harmonics of the magnetic field distribution belonging to the set P_a corresponding to the MMF harmonics of the winding “a”.

The formula for the winding “a” flux linkage in the zero current state can be derived by substituting into Formula (19) the function of the flux density distribution caused by PM for a machine with an asymmetric rotor (14). After performing formal mathematical transformations, according to [37], the following relationship is obtained for $a = 1, 2, 3$:

$$\psi_{PMa}(\varphi) = \sum_{\zeta \in Q} \sum_{k \in K} \sum_{m \in M_\delta} \sum_{n \in N_\delta} \psi_{\zeta, k, m, n}^{PMa} \cdot e^{-j(\zeta+k+m)x_a} e^{j(-\zeta-k+n)\varphi} \quad (22)$$

where

$$\psi_{\zeta, k, m, n}^{PMa} = \begin{cases} 2 r_s l_c B_\zeta^m D_k^{PM} \frac{\lambda_{m,n}^\delta}{\lambda_g} W_{\zeta+k+m}^a & \text{for } (\zeta+k) \neq 0 \wedge (\zeta+k+m) \in P_a \\ 0 & \text{for opposed condition} \end{cases} \quad (23)$$

The EMF of the “a” winding can be written using Formulas (22) and (23), presenting the flux linkage of the PM machine in a current state

$$e_{PMa}(\varphi) = -\text{Imag} \left\{ \sum_{\zeta \in Q} \sum_{k \in K} \sum_{m \in M_\delta} \sum_{n \in N_\delta} EMF_{\zeta, k, m, n}^{PMa} \cdot e^{-j(\zeta+k+m)x_a} e^{j(-\zeta-k+n)\varphi} \right\} \quad (24)$$

where

$$EMF_{\zeta, k, m, n}^{PMa} = \begin{cases} (-\zeta - k + n) \omega 2 r_s l_c B_\zeta^m D_k^{PM} \frac{\lambda_{m,n}^\delta}{\lambda_g} W_{\zeta+k+m}^a & \text{for } (\zeta+k) \neq 0 \wedge (\zeta+k+m) \in P_a \\ 0 & \text{for opposed condition} \end{cases} \quad (25)$$

Generally, in the case of rotor asymmetry, the winding “a” flux linkage caused by PMs and EMF can be presented in the form of a quadruple Fourier series. In the case of stator winding symmetry, the number of turns $w_a = w_b = w_s$, winding factors $k_{wa}^{|\nu|} = k_{wb}^{|\nu|} = k_{ws}^{|\nu|}$, $W_\nu^a = W_\nu^b = W_\nu^s = \frac{w_s k_{ws}^{|\nu|}}{|\nu|}$, and Fourier distribution coefficients of flux linkage and EMF can be simplified: $\psi_{\zeta, k, m, n}^{PMa} = \psi_{\zeta, k, m, n}^{PMs}$, $EMF_{\zeta, k, m, n}^{PMa} = EMF_{\zeta, k, m, n}^{PMs}$ for $a = 1, 2, 3$.

3. Discussion

The steady state is considered when the angular velocity of the rotor is constant $\omega = \Omega$ and then $\varphi = \Omega \cdot t$. The individual frequencies of the bands contained in the EMF spectrum in steady state are determinable using a mathematical model according to Formulas (24) and (25). For this purpose, it is necessary to know the content of harmonic sets for the distributions of functions, including MMF, air gap flux density, and unit air gap permeance, that satisfy the conditions $(\zeta + k + m) \in P_a \wedge (\zeta + k) \neq 0 \wedge (-\zeta - k + n) \neq 0$.

The content of MMF harmonic sets are as follows:

$P_a = \{\dots - 5p, -3p, -p, p, 3p, 5p \dots\}$ —winding with the integer number of slots per pole and phase; $P_a = \{\dots - 5p, -4p, -3p, -2p, -p, p, 2p, 3p, 4p, 5p \dots\}$ —winding with a fractional number of slots per pole and phase.

The content of flux density harmonic sets are as follows:

$\zeta \in Q = \{\dots - 5p, -3p, -p, p, 3p, 5p \dots\}; k \in K = \{\dots - 3, -2, -1, 0, 1, 2, 3 \dots\}$.

The content of unit permeance function harmonic sets M_δ, N_δ for cases of symmetry and eccentricity can be determined as follows:

- Symmetry of magnetic circuit $m = \pm h_1 \cdot z_s; n = 0$;
- Static eccentricity of rotor $m = \pm h_1 \cdot z_s \pm h_2; n = 0$;
- Dynamic eccentricity of rotor $m = \pm h_1 \cdot z_s \pm h_2; n = \mp h_2$;
- Mixed eccentricity of rotor; $m = \pm h_1 \cdot z_s \pm h_2; n = \pm h_2$.

Here, z_s —number of stator slots and $h_1, h_2 = 0, 1, 2, \dots$

Taking into account the assumed content of the harmonic sets of the distribution of functions MMF, flux density, and unit air gap permeance, it is possible to compare the harmonics occurring in the EMF for various cases of rotor failure. A general relationship expressing the EMF at steady state is presented as follows:

$$e_{PMa}(t) = \sum_{\zeta} \underline{EMF}_{\zeta}^{PMa} \cdot e^{j\zeta \Omega t} \tag{26}$$

The EMF pulsations for particular cases of rotor faults are listed in Table 1.

Table 1. EMF pulsations for individual cases of rotor faults.

Type of Rotor Fault	Stator Winding with the Integer Number Slots per Pole and Phase	Stator Winding with the Fractional Number Slots per Pole and Phase
PM without demagnetization (no PM damage)		
Symmetry no PM demagnetization	$\zeta = \pm(2h_1 - 1)p$	$\zeta = \pm(2h_1 - 1)p$
Static eccentricity no PM demagnetization	$\zeta = \pm(2h_1 - 1)p$	$\zeta = \pm(2h_1 - 1)p$
Dynamic eccentricity no PM demagnetization	$\zeta = \pm(2h_1 - 1 \pm \frac{h_2 z_s}{p})p$	$\zeta = \pm(2h_1 - 1 \pm \frac{h_2 z_s}{p})p$
Mixed eccentricity no PM demagnetization	$\zeta = \pm(2h_1 - 1 \pm \frac{h_2}{p})p$	$\zeta = \pm(2h_1 - 1 \pm \frac{h_2}{p})p$
PM with demagnetization (PM damage)		
Symmetry with PM demagnetization	$\zeta = \pm(2h_1 - 1 \pm \frac{h_2 z_s}{p})p$	$\zeta = \pm(h_1 \pm \frac{h_2 z_s}{p})p$
Static eccentricity with PM demagnetization	$\zeta = \pm(2h_1 - 1 \pm \frac{h_2}{p})p$	$\zeta = \pm(h_1 \pm \frac{h_2}{p})p$
Dynamic eccentricity with PM demagnetization	$\zeta = \pm(2h_1 - 1 \pm \frac{h_2 z_s}{p})p$	$\zeta = \pm(h_1 \pm \frac{h_2 z_s}{p})p$
Mixed eccentricity with PM demagnetization	$\zeta = \pm(2h_1 - 1 \pm \frac{h_2}{p})p$	$\zeta = \pm(h_1 \pm \frac{h_2}{p})p$

Here, $h_1 = 1, 2, 3, \dots; h_2 = 0, 1, 2, 3 \dots$

Based on the qualitative analysis of the pulsations of individual EMF harmonics (Table 1), a possible case of rotor faults can be initially qualitatively indicated; however, there are cases of ambiguity, as similar pulsations occur for different cases of rotor faults. It is clearly visible that everything depends on the design of the machine, i.e., primarily, the number of slots in relation to the number of pole pairs and the type of winding characterized by an integer or fractional number of slots per pole and phase.

4. Case Study

4.1. Description of the Tested Machine

The verification of created models was carried out for a PM machine used in a Toyota Prius model 2004. The basic parameters and design data of the machine are summarized according to Table 2.

Table 2. Machine parameters and construction data.

Parameters and Dimensions of the PM Machine
Machine rated data: peak power rating 50 kW (1200 rpm); peak torque rating 400 Nm; voltage constant 1.33 Vrms/Hz; number of pole pairs $p = 4$
Axial length of stator and rotor core $l_c = 83.56$ mm
Stator outer radius 134.62 mm; rotor outer radius $r_r = 80.20$ mm
Stator internal radius $r_s = 80.95$ mm; length of air gap $l_\delta = 0.75$ mm
Single magnet dimensions: 18.00×6.48 mm ($l_m = 6.48$ mm); PM opening angle 145° ; $\beta = 13.6^\circ$
PM residual flux density $B_r = 1.2$ T; PM coercive force $H_c = 904$ kA/m
Winding type—single layer; number of stator slots $z_s = 48$; winding span—6 slots
Number of slots per pole and phase—2
Total number of phase winding turns $w_s = 72$; equivalent slot opening $b_s = 2$ mm

The presented parameters are complemented by the winding coefficients determined for individual harmonics multiplied by the number of pole pairs p (Figure 7).

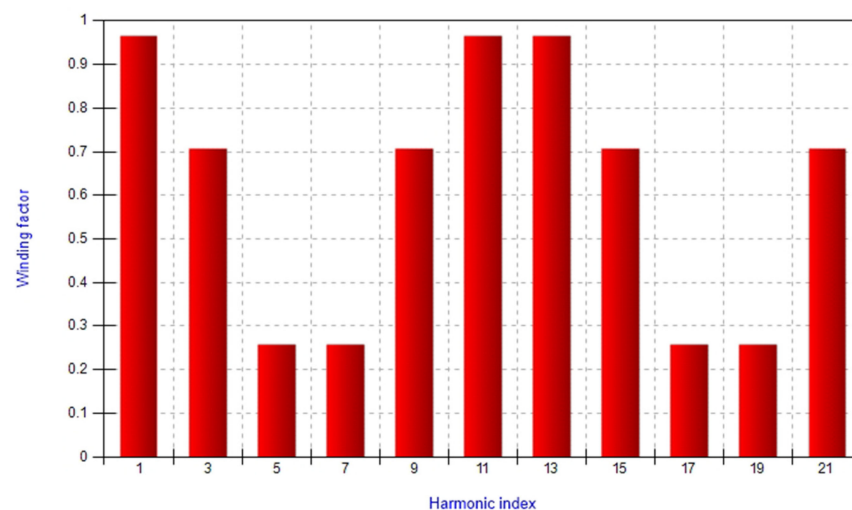


Figure 7. Stator winding factors of an example PM machine according to “ p ” harmonic index.

4.2. Results of Numerical Tests

4.2.1. Permeance Function

First, the distributions of the unit permeance function were analyzed for the case of symmetry of the magnetic circuit and asymmetry of the magnetic circuit related to

the occurrence of rotor eccentricity (static, dynamic, and mixed, where the level of eccentricity is defined as $\varepsilon_s = d_s/l_\delta, \varepsilon_d = d_d/l_\delta$). The distribution coefficients for this function were determined using the formulas in Appendix A. The air gap permeance function $\lambda_\delta(x, \varphi) = \sum_{m \in M_\delta} \sum_{n \in N_\delta} \lambda_{m,n}^\delta e^{jm_x} e^{jn_\varphi}$ in cases of symmetry and rotor eccentricity is presented in Figure 8.

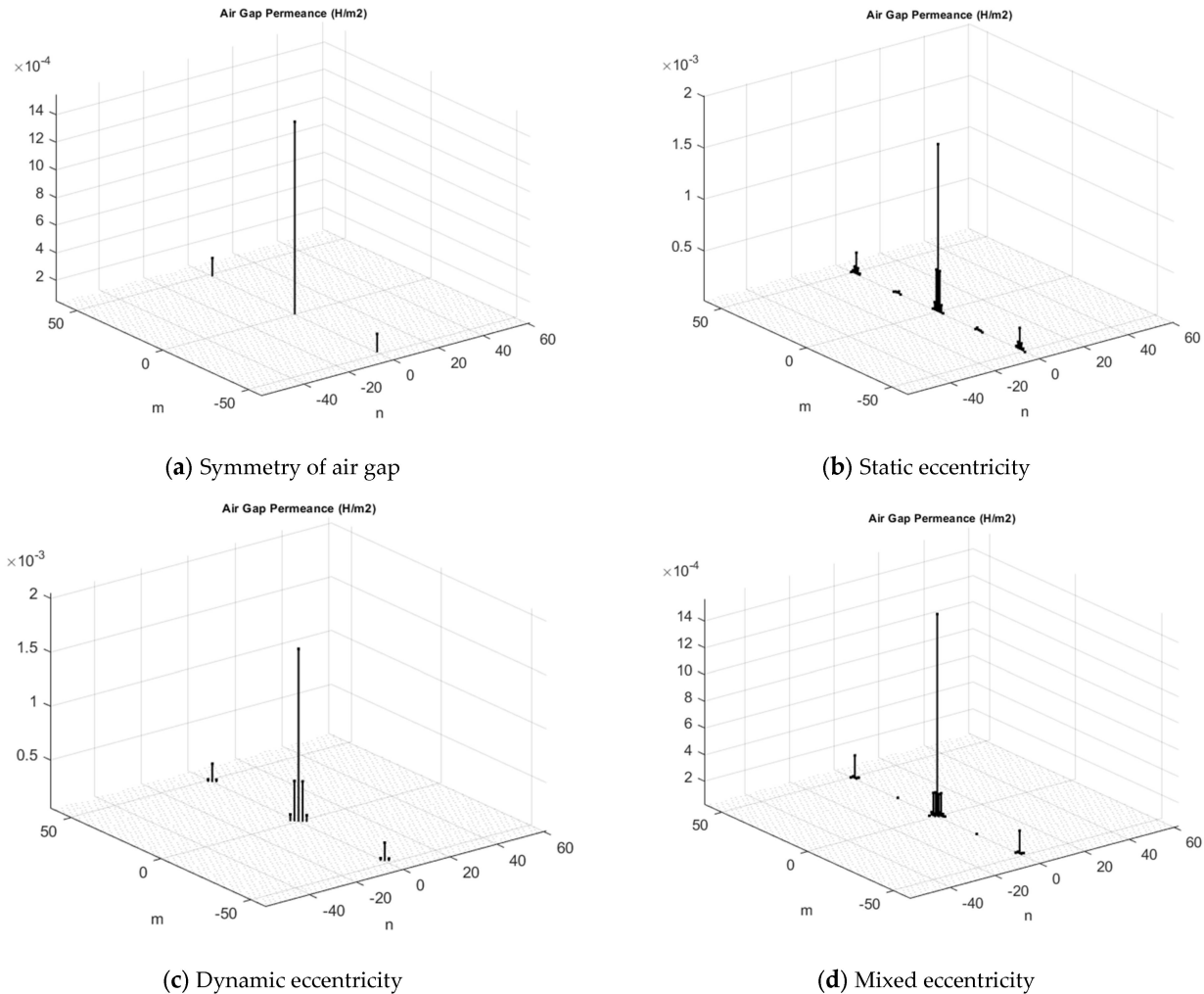
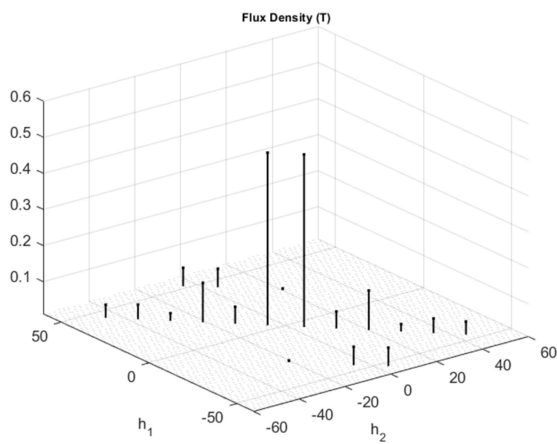


Figure 8. Permeance function: (a) full air-gap symmetry; (b) static eccentricity $\varepsilon_s = 0.2$; (c) dynamic eccentricity $\varepsilon_d = 0.2$; and (d) mixed eccentricity $\varepsilon_s = 0.2$ and $\varepsilon_d = 0.2$.

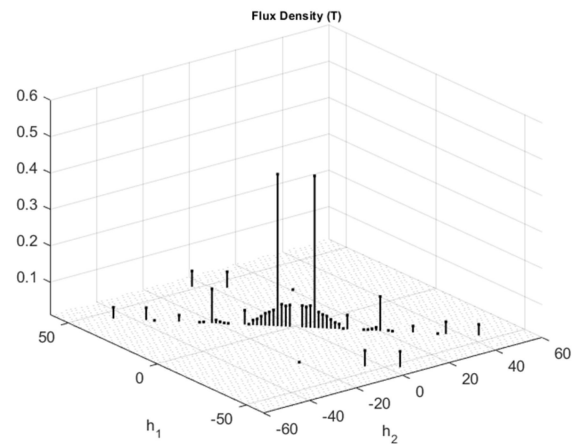
Analyzing the decomposition of the permeance function, it can be seen that the side bands are arranged in accordance with the characteristic features. For the case of static eccentricity, the distribution is along the column (it does not depend on the rotation angle), and for dynamic eccentricity, it is distributed along the diagonals. Mixed eccentricity is a composite of these distributions and it can be seen that certain harmonic clusters are created around the fundamental (zero) and slot harmonics.

4.2.2. Air-Gap Flux Density

The next tests concerned the decomposition of the air-gap flux density. The spectra of flux density $B_{PM}(x, \varphi) = \sum_{h_1} \sum_{h_2} B_{h_1, h_2}^{PM} e^{jh_1 x} e^{jh_2 \varphi}$ in cases of rotor eccentricity and PM damage (one PM pole demagnetization) determined in accordance with the analytical formulas presented earlier are presented in Figures 9–12 for the analyzed cases of rotor failure.

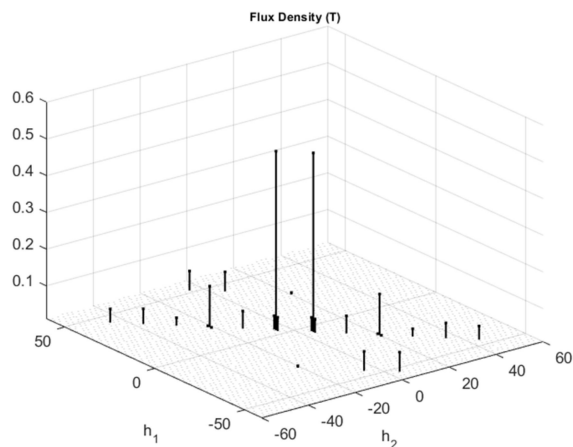


(a) Symmetry of air-gap (no PM damage)

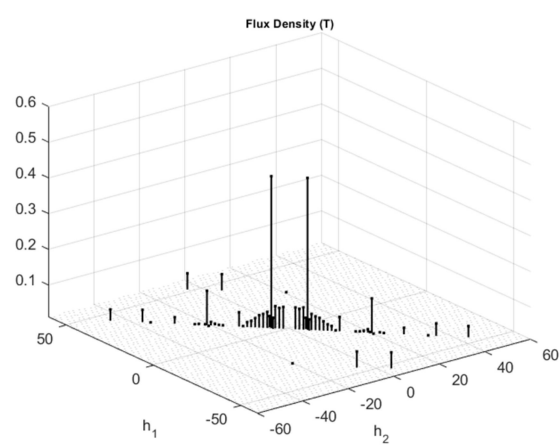


(b) PM magnetic pole damage without eccentricity

Figure 9. Flux density: (a) symmetry of air-gap; (b) symmetry of air-gap and PM demagnetization.

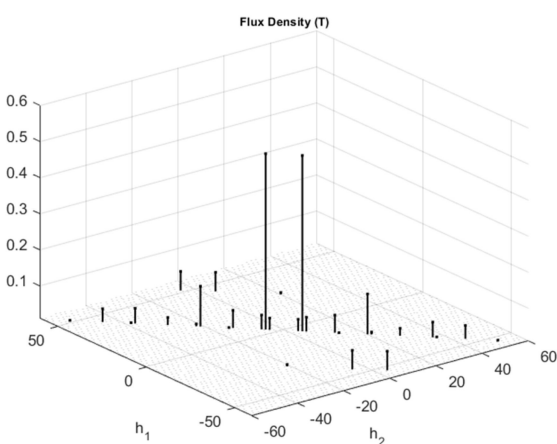


(a) Static eccentricity (no PM damage)

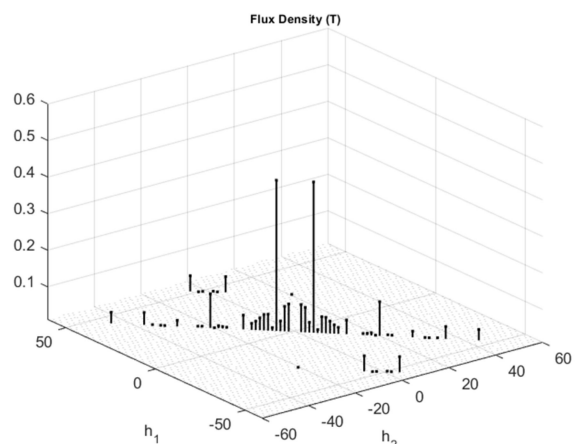


(b) PM magnetic pole damage with static eccentricity

Figure 10. Flux density: (a) static eccentricity ($\epsilon_s = 0.2$); (b) static eccentricity ($\epsilon_s = 0.2$) and PM demagnetization.



(a) Dynamic eccentricity (no PM damage)



(b) PM magnetic pole damage with dynamic eccentricity

Figure 11. Flux density: (a) dynamic eccentricity ($\epsilon_d = 0.2$); (b) dynamic eccentricity ($\epsilon_d = 0.2$) and PM demagnetization.

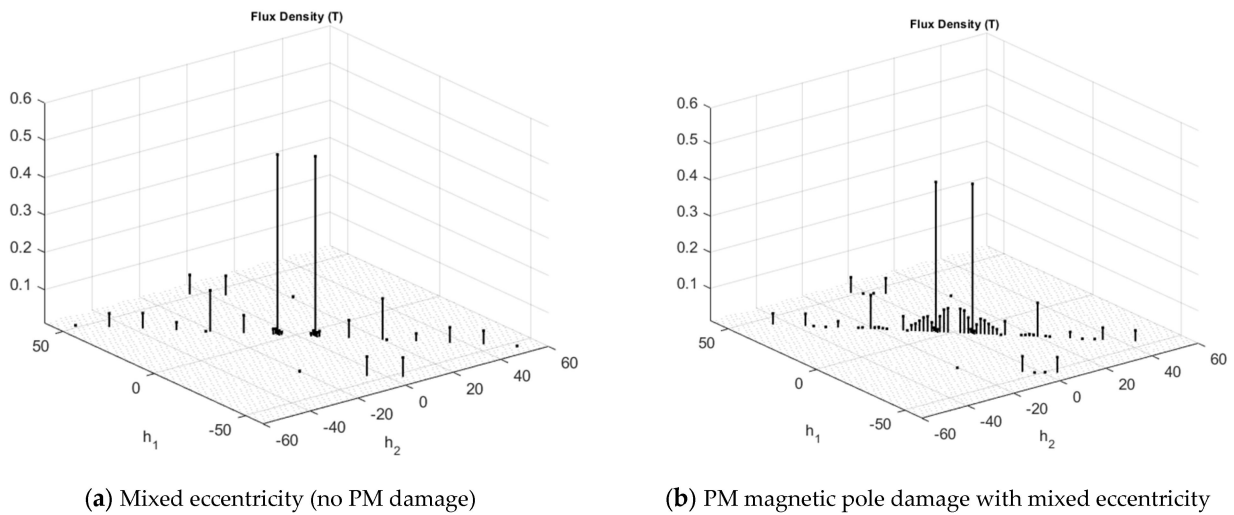


Figure 12. Flux density: (a) mixed eccentricity ($\epsilon_s = 0.1$ and $\epsilon_d = 0.1$); (b) mixed eccentricity ($\epsilon_s = 0.1$ and $\epsilon_d = 0.1$) and PM demagnetization.

Specific features of the arrangement of the bands can also be noticed in the air gap flux density distributions. The cases of simultaneous occurrence of magnetic core asymmetry and PM demagnetization require special emphasis. The occurrence of PM demagnetization is visible in a characteristic ridge along the diagonal. The above comparison shows that individual cases of rotor failure significantly enrich the spectrum of flux density distribution in the air gap compared to a machine without failure (symmetry).

4.2.3. Electromotive Force

The tests were carried out for a Prius electric motor model operating in the generator state without load in order to determine the harmonic content in the EMF waveforms. The tests were performed for a steady state at a speed of $\Omega = 1200$ rpm, which corresponds to a frequency of 80 Hz of EMF waveforms. Verifications were based on FEM analysis using Simcenter MAGNET software (Version 2020.1.0.35).

Figure 13 shows a cross-section of the symmetrical machine and example calculations of the magnetic field distribution in the zero current state.

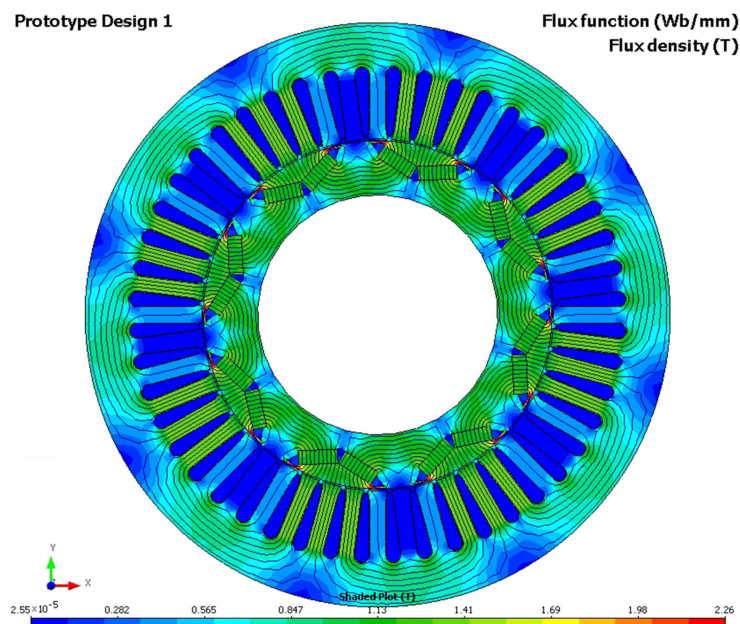


Figure 13. Example FEM calculations of flux density distribution.

Tests using analytical and field models (FEM) allowed for the determination of induced EMFs in the phases of the stator winding for cases of symmetry and eccentricity with the simultaneous occurrence of PM demagnetization damage. The effective values (RMS) of the induced EMF of the stator winding were subjected to preliminary verification. The results are summarized in Table 3.

Table 3. RMS values of phase-back EMF for the example machine ($\Omega = 1200$ rpm; $f = 80$ Hz).

Type of Rotor Fault	PM without Demagnetization (No PM Damage) EMF (RMS)			PM with Demagnetization (PM Damage) EMF (RMS)		
	Analytical Formulas	FEM Calculations	$ \Delta\text{EMF} (\%) $	Analytical Formulas	FEM Calculations	$ \Delta\text{EMF} (\%) $
Symmetry of air gap	81.9 V	83.6 V	2.4%	71.6 V	74.0 V	3.2%
Static eccentricity	83.5 V	82.7 V	1.0%	73.0 V	73.2 V	0.3%
Dynamic eccentricity	83.5 V	83.7 V	0.2%	71.8 V	74.2 V	3.2%
Mixed eccentricity	82.7 V	83.6 V	1.1%	72.3 V	74.0 V	3.3%

The satisfactory percentage differences $|\Delta\text{EMF} (\%)|$ presented in Table 3 between the results obtained on the basis of the proposed mathematical formulas and field calculations (max. 3.3%) confirm their good convergence and, therefore, the correctness of the analytical model. By measuring the effective value of the phase voltage in a zero current state, it is possible to initially detect PM demagnetization damage, which is an obvious matter, but the rotor eccentricity could not be detected. In our case, damage to one pole of the magnets led to a more than 10% reduction in the effective EMF value.

Further tests of the correctness and usefulness of the analytical model included quantitative and qualitative analyses of the content of higher harmonics in the EMF spectra. Figures 14–17 show the obtained results. The presented spectra (in dB) are for the adopted reference level 1 mV. The results of EMF calculations are marked with dashed lines with the marker “o” for analytical model, while FEM analyses are shown with a solid line.

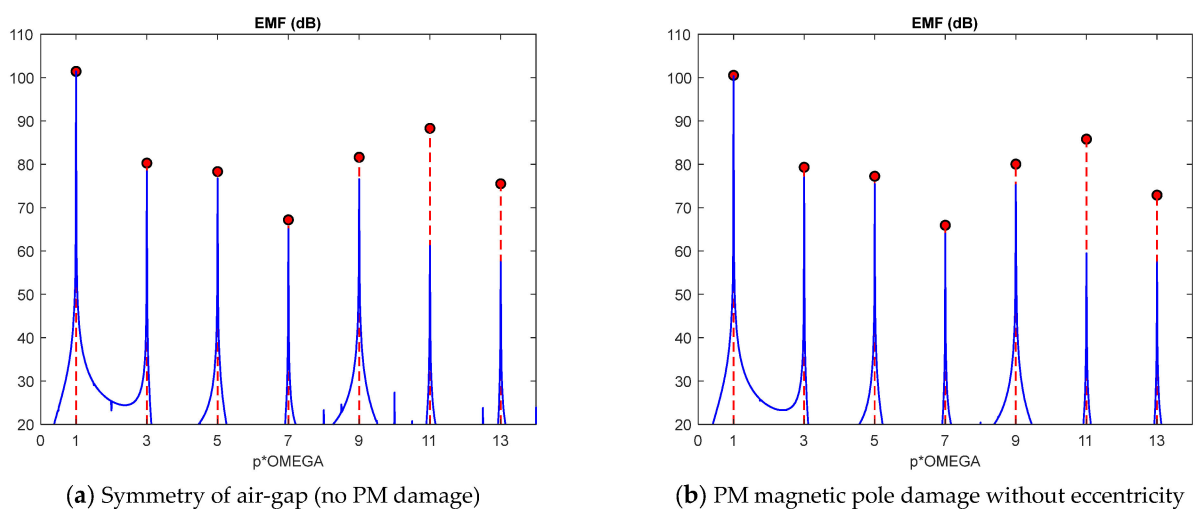


Figure 14. Stator phase back EMF: (a) air-gap symmetry; (b) air-gap symmetry and PM demagnetization (analytical calculations—dashed line ending with the marker “o”; FEM analysis—solid line).

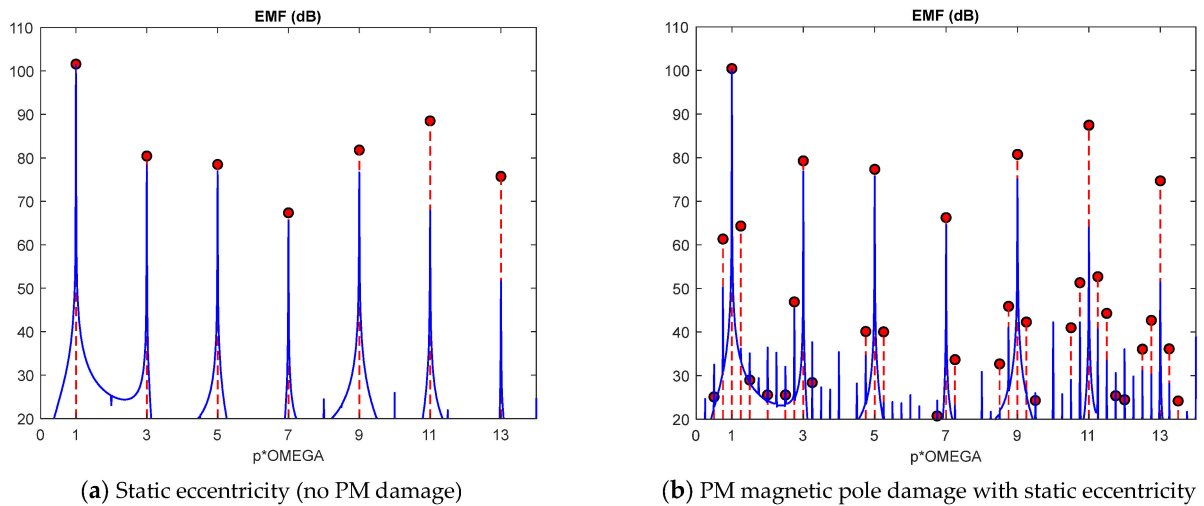


Figure 15. Stator phase back EMF: (a) static eccentricity ($\varepsilon_s = 0.2$); (b) static eccentricity ($\varepsilon_s = 0.2$) and PM demagnetization (analytical calculations—dashed line ending with the marker “o”; FEM analysis—solid line).

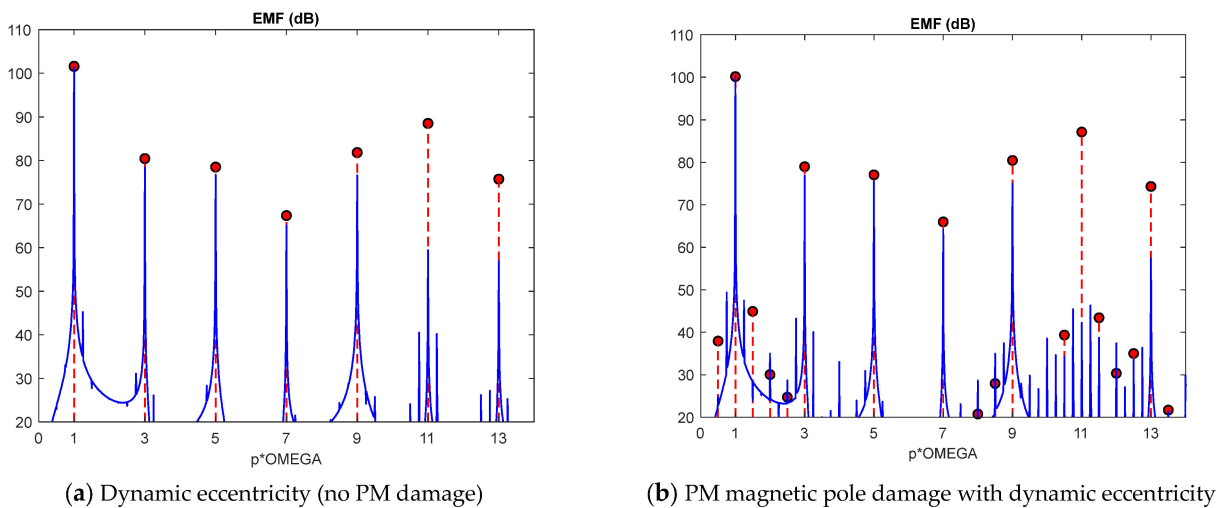


Figure 16. Stator phase back EMF: (a) dynamic eccentricity ($\varepsilon_d = 0.2$); (b) dynamic eccentricity ($\varepsilon_d = 0.2$) and PM demagnetization (analytical calculations—dashed line ending with the marker “o”; FEM analysis—solid line).

The preliminary analyses of the bands obtained for the EMF distributions show good qualitative and satisfactory quantitative convergence of the results. However, some discrepancies appear in the higher harmonics of the spectrum. The authors’ previous doubts are clearly confirmed. For the analyzed machine structure, the influence of single damages is not visible, except for the case of mixed eccentricity. From a practical point of view, in this machine, PM demagnetization and static and dynamic eccentricities are undetectable. The spectrum becomes richer for the simultaneous occurrence of PM demagnetization and static or dynamic eccentricity. Additional bands appear in the spectrum, which may be characteristic of rotor failure; however, they are at a very low level. This is confirmed by the EMF harmonics listed in Table 4 for the analyzed example machine.

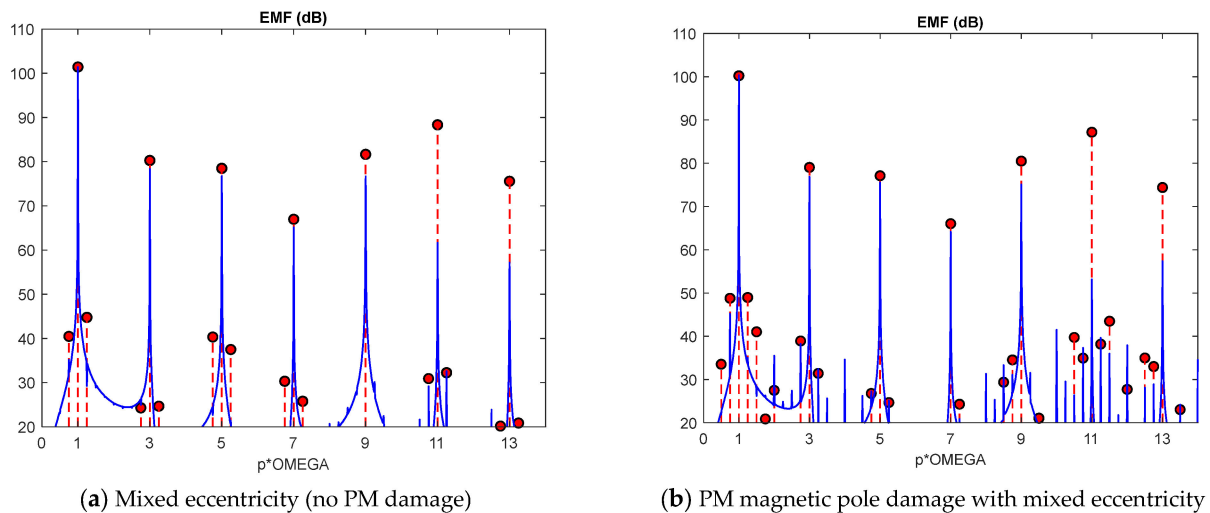


Figure 17. Stator phase back EMF: (a) mixed eccentricity ($\epsilon_s = 0.1$ and $\epsilon_d = 0.1$); (b) mixed eccentricity ($\epsilon_s = 0.1$ and $\epsilon_d = 0.1$) and PM demagnetization (analytical calculations—dashed line ending with the marker “o”; FEM analysis—solid line).

Table 4. EMF pulsations for the example machine.

Type of Rotor Fault	EMF Pulsations	
	PM without Demagnetization (no PM Damage)	PM with Demagnetization (PM Damage)
Symmetry	$\zeta = \pm p, \pm 3p, \pm 5p \dots$	$\zeta = \pm p, \pm 3p, \pm 5p \dots$
Static eccentricity	$\zeta = \pm p, \pm 3p, \pm 5p \dots$	$\zeta = \pm(2h_1 - 1 \pm \frac{h_2}{p})p$
Dynamic eccentricity	$\zeta = \pm p, \pm 3p, \pm 5p \dots$	$\zeta = \pm p, \pm 3p, \pm 5p \dots$
Mixed eccentricity	$\zeta = \pm(2h_1 - 1 \pm \frac{h_2}{p})p$	$\zeta = \pm(2h_1 - 1 \pm \frac{h_2}{p})p$

Here, $h_1 = 1, 2, 3, \dots$; $h_2 = 0, 1, 2, 3, \dots$

To sum up, it should be added that the detection of particular cases of rotor damage will require, in addition to qualitative analyses of the EMF spectrum, quantitative analyses as well, but this is not easy due to the relatively low level of changes in the amplitude values.

5. Conclusions

The proposed mathematical model allowing for the determination of harmonics in the EMF spectrum of a PM machine with internal magnets is not very sophisticated. It is based on the analysis of the effects of spatial harmonics of the magnetic field in the air gap of the machine. Its advantage is that it is sufficiently accurate and the time to obtain results is practically instantaneous (a few seconds on a PC), while FEM analyses are very time-consuming (on a good workstation it took almost 24 h for one case). Moreover, FEM analyses did not enable the synthesis of electromagnetic phenomena occurring in the machine. The parameters of the created analytical model had integral forms, so the accuracy of the results is limited. There are, of course, discrepancies between the results obtained from the analytical model and FEM, although the basic bands are almost identical. Another advantage of the presented model is that it takes into account the design features of the machine (number of stator slots, pole pairs, arrangement of magnets, etc.) and assigns spectrum bands to failure cases.

Some of the authors’ doubts were confirmed. This was confirmed by the results of EMF spectrum analyses for an example machine (Toyota Prius), for which practically pure cases of single damage did not introduce additional components in the EMF spectrum compared to the state without damage (symmetry). It can therefore be concluded that for example machine structure, the single damages should be undetectable by EMF harmonic

analysis. Analyzing the results, it can be said that the harmonic amplitude values appearing in the EMF spectrum as a result of damage are at a very low level, which obviously makes the process of recognizing and diagnosing particular cases much more difficult.

The presented methodology can be used to quickly and easily create patterns and symptoms of damage that can be implemented in the control system of a power electronic converter cooperating with a machine. A modern electric drive system is usually equipped with fast voltage sensors, the signals of which are sent via ADC converter systems to be processed by a microprocessor system. During the operation of the drive system, based on a simple voltage measurement in the no-current state, the microprocessor system can recreate the distribution of the electromagnetic field, perform its spectral analysis, and compare it with a saved standard. A practical aspect of using the methodology presented in the article is the creation of spectrum patterns based on which the drive's microprocessor system can indicate in real time the nature of the failure.

Author Contributions: Conceptualization, N.R.-P. and T.W.; methodology N.R.-P. and T.W.; validation, N.R.-P. and T.W.; investigation, N.R.-P. and T.W.; data curation, N.R.-P. and T.W.; writing—original draft preparation, N.R.-P. and T.W.; writing—review and editing, N.R.-P. and T.W.; supervision, N.R.-P. and T.W. All authors have read and agreed to the published version of the manuscript.

Funding: The work presented in this paper was funded by subsidies for science granted by the Polish Ministry of Science and Higher Education for Cracow University of Technology.

Data Availability Statement: Data are contained within the article.

Conflicts of Interest: The authors declare no conflict of interest.

Appendix A

The lengths of the magnetic field lines in the air gap $\delta(x, \varphi)$ in cases of eccentricity can be approximated using the sum of the segments AB and BC, according to Figure A1.

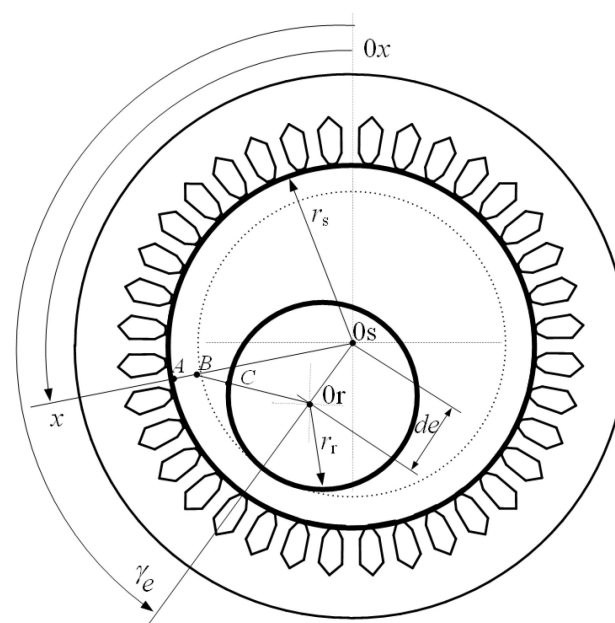


Figure A1. Simplified cross-section of the machine with rotor eccentricity.

This approach allows us to take into account the condition of the perpendicular direction of entry and exit of these lines from the surfaces of the iron cores of the stator and rotor. Formally, it can be written as follows:

$$\delta(x, \varphi) = r_s - 2r_r - d_e + \sqrt{[(r_r + d_e) \cos x - d_e \cos \gamma_e]^2 + [(r_r + d_e) \sin x - d_e \sin \gamma_e]^2} \quad (\text{A1})$$

Parameters d_e and γ_e in Figure 10 are determined by parameters given as follows:

- For static eccentricity:

$$d_e = d_s, d_d = 0, \gamma_e = \gamma = \text{const.} \quad (\text{A2})$$

- For dynamic eccentricity:

$$d_e = d_d, d_s = 0, \gamma_e = \varphi \quad (\text{A3})$$

- For mixed eccentricity:

$$\begin{aligned} d_s \neq 0, d_d \neq 0, \gamma = \text{const} \\ d_e = d(\varphi) = \sqrt{d_s^2 + d_d^2 + 2d_s d_d \cos(\varphi - \gamma)} \\ \gamma_e = \arcsin\left(\frac{d_d}{d_e} \sin(\varphi - \gamma)\right) \quad \text{for } d_e \neq 0 \end{aligned} \quad (\text{A4})$$

Appendix B

The values of corrections $\Delta\delta_{\max}(x, \varphi)$ depend on radial coordinate r , for which the distribution of the magnetic field is analyzed [35,36,40]. In the general case, a good approximation is the cylindrical stator surface; therefore, $r = r_s$. The equivalent length of the magnetic flux lines can be determined locally for any position of the rotor φ

$$\Delta\delta_{\max}(x, \varphi) = \delta(x, \varphi) \cdot \left\{ \sqrt{1 + \left(\frac{b_s}{2\delta(x, \varphi)}\right)^2 \cdot (1 + v(r)^2)} - 1 \right\} \quad (\text{A5})$$

$v(r)$ —the factor is calculated for a particular value of the r radial coordinate according to [35,36,40] by solving the following non-linear equation:

$$\begin{aligned} (r - r_r) \frac{\pi}{b_s} - \frac{1}{2} \ln \left(\frac{\sqrt{\left(1 + \left(\frac{2\delta(x, \varphi)}{b_s}\right)^2\right)^2 + v(r)^2 + v(r)}}{\sqrt{\left(1 + \left(\frac{2\delta(x, \varphi)}{b_s}\right)^2\right)^2 + v(r)^2 - v(r)}} \right) + \\ + \frac{2\delta(x, \varphi)}{b_s} \arctan \left(\frac{2\delta(x, \varphi)}{b_s} \frac{v(r)}{\sqrt{\left(1 + \left(\frac{2\delta(x, \varphi)}{b_s}\right)^2\right)^2 + v(r)^2}} \right) = 0 \end{aligned} \quad (\text{A6})$$

References

1. Hsu, J.S.; Ayers, C.W.; Coomer, C.L. *Report on Toyota/Prius Motor Design and Manufacturing Assessment*; Oak Ridge National Laboratory: Oak Ridge, TN, USA, 2004; ORNL/TM-2004/137.
2. Hsu, J.S.; Ayers, C.W.; Coomer, C.L.; Wiles, R.H.; Campbell, S.L.; Lowe, K.T.; Michelhaugh, R.T. *Report on Toyota/Prius Motor Torque Capability, Torque Property, No-Load Back EMF and Mechanical Losses*; Oak Ridge National Laboratory: Oak Ridge, TN, USA, 2004; ORNL/TM-2004/185.
3. Ayers, C.W.; Hsu, J.S.; Marlino, L.D.; Miller, C.W.; Ott, G.W.; Oland, C.B. *Evaluation of 2004 Toyota Prius Hybrid Electric Drive System Interim Report*; Oak Ridge National Laboratory: Oak Ridge, TN, USA, 2004; ORNL/TM-2004/247.
4. Loganayaki, A.; Kumar, R.B. Permanent Magnet Synchronous Motor for Electric Vehicle Applications. In Proceedings of the 5th International Conference on Advanced Computing & Communication Systems (ICACCS), Coimbatore, India, 15–16 March 2019; pp. 1064–1069. [CrossRef]
5. Jha, D.K.; Jain, A. Advancements in electric motor technology: A review of emerging trends and future prospects. *Int. J. Comput. Sci. Inf. Syst.* **2023**, *8*, 5–8. Available online: <https://scientiamresearch.org/index.php/ijcsis/article/view/10> (accessed on 29 April 2024).
6. Ruoqiong, L.; Zonglin, W.; Li, X. Review on fault diagnosis and active fault tolerant control of permanent magnet synchronous motor drive system. *J. Appl. Sci. Eng.* **2021**, *24*, 185–205. [CrossRef]
7. Ismagilov, F.R.; Vavilov, V.Y.; Ayguzina, V.V. Method for diagnostic of permanent-magnet electrical machines. *Chem. Technol. Control. Manag.* **2018**, *2018*, 25. [CrossRef]

8. Park, Y.; Yang, C.; Lee, S.B.; Lee, D.M.; Fernandez, D.; Reigosa, D.; Briz, F. Online Detection and Classification of Rotor and Load Defects in PMSMs Based on Hall Sensor Measurements. *IEEE Trans. Ind. Appl.* **2019**, *55*, 3803–3812. [[CrossRef](#)]
9. Cheng, M.; Hang, J.; Zhang, J. Overview of fault diagnosis theory and method for permanent magnet machine. *Chin. J. Electr. Eng.* **2015**, *1*, 21–36. [[CrossRef](#)]
10. Zheng, J.; Wang, Z.; Wang, D.; Li, Y.; Li, M. Review of fault diagnosis of PMSM drive system in electric vehicles. In Proceedings of the 36th Chinese Control Conference (CCC), Dalian, China, 26–28 July 2017; pp. 7426–7432. [[CrossRef](#)]
11. Alvarez-Gonzalez, F.; Griffo, A.; Sen, B.; Wang, J. Real-Time Hardware-in-the-Loop Simulation of Permanent-Magnet Synchronous Motor Drives Under Stator Faults. *IEEE Trans. Ind. Electron.* **2017**, *64*, 6960–6969. [[CrossRef](#)]
12. Chen, Y.; Liang, S.; Li, W.; Liang, H.; Wang, C. Faults and Diagnosis Methods of Permanent Magnet Synchronous Motors: A Review. *Appl. Sci.* **2019**, *9*, 2116. [[CrossRef](#)]
13. Liang, H.; Chen, Y.; Liang, S.; Wang, C. Fault Detection of Stator Inter-Turn Short-Circuit in PMSM on Stator Current and Vibration Signal. *Appl. Sci.* **2018**, *8*, 1677. [[CrossRef](#)]
14. Shen, T.; Kilic, A.; Thulfaut, C.; Reuss, H.-C. An Intelligent Diagnostic Method for Permanent Magnet Synchronous Motors (PMSM) in the Electric Drive of Autonomous Vehicles. In Proceedings of the 2019 21st European Conference on Power Electronics and Applications (EPE '19 ECCE Europe), Genova, Italy, 3–5 September 2019; pp. 1–10. [[CrossRef](#)]
15. Pietrzak, P.; Wolkiewicz, M. Comparison of Selected Methods for the Stator Winding Condition Monitoring of a PMSM Using the Stator Phase Currents. *Energies* **2021**, *14*, 1630. [[CrossRef](#)]
16. Pietrzak, P.; Wolkiewicz, M. Demagnetization Fault Diagnosis of Permanent Magnet Synchronous Motors Based on Stator Current Signal Processing and Machine Learning Algorithms. *Sensors* **2023**, *23*, 1757. [[CrossRef](#)]
17. Moosavi, S.S.; Djerdir, A.; Amirat, Y.A.; Khaburi, D.A. Demagnetization fault diagnosis in permanent magnet synchronous motors: A review of the state-of-the-art. *J. Magn. Magn. Mater.* **2015**, *391*, 203–212. [[CrossRef](#)]
18. Urresty, J.-C.; Riba, J.-R.; Romeral, L. A Back-EMF Based Method to Detect Magnet Failures in PMSMs. *IEEE Trans. Magn.* **2013**, *49*, 591–598. [[CrossRef](#)]
19. Alameh, K.; Cité, N.; Hoblos, G.; Barakat, G. Vibration-based Fault Diagnosis Approach for Permanent Magnet Synchronous Motors. *IFAC-PapersOnLine* **2015**, *48*, 1444–1450. [[CrossRef](#)]
20. Riba Ruiz, J.-R.; Rosero, J.A.; Garcia Espinosa, A.; Romeral, L. Detection of Demagnetization Faults in Permanent-Magnet Synchronous Motors Under Nonstationary Conditions. *IEEE Trans. Magn.* **2009**, *45*, 2961–2969. [[CrossRef](#)]
21. Rasid, S.A.; Gyftakis, K.N.; Mueller, M. Comparative Investigation of Three Diagnostic Methods Applied to Direct-Drive Permanent Magnet Machines Suffering from Demagnetization. *Energies* **2023**, *16*, 2767. [[CrossRef](#)]
22. Skowron, M.; Orłowska-Kowalska, T.; Kowalski, C.T. Detection of Permanent Magnet Damage of PMSM Drive Based on Direct Analysis of the Stator Phase Currents Using Convolutional Neural Network. *IEEE Trans. Ind. Electron.* **2022**, *69*, 13665–13675. [[CrossRef](#)]
23. Akar, M.; Eker, M. Demagnetization Fault Diagnosis in Permanent Magnet Synchronous Motors. *Przegład Elektrotech.* **2013**, *89*, 229–233.
24. Li, Z.; Wu, Q.; Yang, S.; Chen, X. Diagnosis of rotor demagnetization and eccentricity faults for IPMSM based on deep CNN and image recognition. *Complex Intell. Syst.* **2022**, *8*, 5469–5488. [[CrossRef](#)]
25. Gyftakis, K.N.; Skarmoutsos, G.A.; Barajas-Solano, I.; Burchell, J.; Mueller, M. Critical Aspects of Demagnetization Faults in Multi-Stage Direct Drive Permanent Magnet Generators for Renewables. *IEEE Trans. Ind. Appl.* **2023**, *59*, 6655–6663. [[CrossRef](#)]
26. Gyftakis, K.N.; Rasid, S.A.; Skarmoutsos, G.A.; Mueller, M. The Demagnetization Harmonics Generation Mechanism in Permanent Magnet Machines with Concentrated Windings. *IEEE Trans. Energy Convers.* **2021**, *36*, 2934–2944. [[CrossRef](#)]
27. Ebrahimi, B.M.; Javan Roshtkhari, M.; Faiz, J.; Khatami, S.V. Advanced Eccentricity Fault Recognition in Permanent Magnet Synchronous Motors Using Stator Current Signature Analysis. *IEEE Trans. Ind. Electron.* **2014**, *61*, 2041–2052. [[CrossRef](#)]
28. Ebrahimi, B.M.; Faiz, J.; Araabi, B.N. Pattern identification for eccentricity fault diagnosis in permanent magnet synchronous motors using stator current monitoring. *IET Electr. Power Appl.* **2010**, *4*, 418–430. [[CrossRef](#)]
29. Ma, C.; Gao, Y.; Degano, M.; Wang, Y.; Fang, J.; Gerada, C.; Zhou, S.; Mu, Y. Eccentric position diagnosis of static eccentricity fault of external rotor permanent magnet synchronous motor as an in-wheel motor. *IET Electr. Power Appl.* **2020**, *14*, 2263–2272. [[CrossRef](#)]
30. Le Roux, W.; Harley, R.G.; Habetler, T.G. Detecting Rotor Faults in Low Power Permanent Magnet Synchronous Machines. *IEEE Trans. Power Electron.* **2007**, *22*, 322–328. [[CrossRef](#)]
31. Goktas, T.; Zafarani, M.; Akin, B. Separation of broken magnet and static eccentricity failures in PMSM. In Proceedings of the IEEE International Electric Machines & Drives Conference (IEMDC), Coeur d'Alene, ID, USA, 10–13 May 2015; pp. 1459–1465. [[CrossRef](#)]
32. Faiz, J.; Exiri, S.A.H. Short-circuit fault diagnosis in permanent magnet synchronous motors—An overview. In Proceedings of the 2015 Intl Aegean Conference on Electrical Machines & Power Electronics (ACEMP), 2015 Intl Conference on Optimization of Electrical & Electronic Equipment (OPTIM) & 2015 Intl Symposium on Advanced Electromechanical Motion Systems (ELECTROMOTION), Side, Turkey, 2–4 September 2015; pp. 18–27. [[CrossRef](#)]
33. Radwan-Pragłowska, N.; Wegiel, T. Permanent Magnet Selections for AFPM Disc Generators. *Energies* **2022**, *15*, 7601. [[CrossRef](#)]
34. Zhu, Z.Q.; Howe, D.; Ekkehard, B.; Ackermann, B. Instantaneous magnetic field distribution in brushless permanent magnet motors, part I: Open-circuit field. *IEEE Trans. Magn.* **1993**, *29*, 124–134. [[CrossRef](#)]

35. Zhu, Z.Q.; Howe, D. Instantaneous magnetic field distribution in brushless permanent magnet motors, part III: Effect of Stator Slotting. *IEEE Trans. Magn.* **1993**, *29*, 143–151. [[CrossRef](#)]
36. Heller, B.; Hamata, V. *Harmonic Field Effect in Induction Machines*; Elsevier Scientific: New York, NY, USA, 1977.
37. Sobczyk, T.J.; Drozdowski, P. Inductances of electrical machine winding with a nonuniform air-gap. *Arch. Elektrotech.* **1993**, *76*, 213–218. [[CrossRef](#)]
38. Sobczyk, T.J.; Weinreb, K.; Węgiel, T.; Sułowicz, M. Theoretical study of effects due to rotor eccentricities in induction motors. In Proceedings of the International Symposium on Diagnostics for Electrical Machines, Power Electronics and Drives (IEEE SDEMPED'99), Gijon, Spain, 1–9 September 1999; pp. 289–295.
39. Sobczyk, T.; Weinreb, K.; Węgiel, T.; Sułowicz, M. Influence of stator and rotor slotting on quantitative prediction of induction motor rotor eccentricity. In Proceedings of the International Symposium on Diagnostics for Electrical Machines, Power Electronics and Drives (IEEE SDEMPED'2001), Grado, Italy, 1–3 September 2001; pp. 429–434.
40. Węgiel, T.; Weinreb, K.; Sułowicz, M. Main inductances of induction motor for diagnostically specialized mathematical models. *Arch. Electr. Eng.* **2010**, *59*, 51–66.

Disclaimer/Publisher's Note: The statements, opinions and data contained in all publications are solely those of the individual author(s) and contributor(s) and not of MDPI and/or the editor(s). MDPI and/or the editor(s) disclaim responsibility for any injury to people or property resulting from any ideas, methods, instructions or products referred to in the content.